



# Scaling features of multimode motions in coupled chaotic oscillators

A.N. Pavlov<sup>a,\*</sup>, O.V. Sosnovtseva<sup>a,b</sup>, E. Mosekilde<sup>b</sup>

<sup>a</sup> *Nonlinear Dynamics Laboratory, Department of Physics, Saratov State University, Astrakhanskaya St. 83, 410026 Saratov, Russia*

<sup>b</sup> *Department of Physics, Technical University of Denmark, 2800 Kgs. Lyngby, Denmark*

Accepted 30 September 2002

Communicated by T. Kapitaniak

## Abstract

Two different methods (the WTMM- and DFA-approaches) are applied to investigate the scaling properties in the return-time sequences generated by a system of two coupled chaotic oscillators. Transitions from twomode asynchronous dynamics (torus or torus–chaos) to different states of chaotic phase synchronization are found to significantly reduce the degree of multiscality. The influence of external noise on the possibility of distinguishing the various chaotic states is considered.

© 2002 Elsevier Science Ltd. All rights reserved.

## 1. Introduction

Synchronization is a fundamental nonlinear phenomenon, and the appearance of various forms of entrainment in systems of coupled oscillators is the subject of intensive research in many areas of science [1–3]. The interactive dynamics of chaotic oscillators is particularly challenging, and a variety of approaches to the study of chaotic synchronization have been developed. Chaotic synchronization may play a significant role in the interaction of biological oscillators such as the insulin producing pancreatic cells or the nephrons of the kidney [3]. At the same time, a variety of applications of this phenomenon for secure communication and for monitoring and control of dynamical systems have been suggested. The notion of chaotic synchronization includes a wide range of phenomena, among which are complete synchronization [4], lag synchronization [5], phase synchronization [6], and generalized synchronization [7]. The distinction among these phenomena reflects the varying degree to which the oscillators adjust their dynamics in accordance with one another. Unlike the classical theory of the entrainment for periodic processes, chaotic synchronization deals with the basic frequencies (if they are distinguished in the dynamics of the systems), with instantaneous phases of the oscillations, or with characteristic temporal scales.

It is well-known that nonlinear dynamical systems can demonstrate a final state behavior that depends on the choice of initial conditions. The phenomenon of multistability is clearly expressed in the synchronization of coupled oscillators that individually follows the period-doubling route to chaos. This is an example of so-called phase multistability: The synchronous solutions have different phase relationships between the oscillations [8]. In particular, if two periodic oscillators with  $n$  subharmonics  $\omega_0/2^n$  ( $n = 1, 2, \dots$ ) of the basic frequency  $\omega_0$  are mutually coupled then the phase difference between the interacting subsystems inside the synchronization region can take  $2^n$  values. Similar effects can be observed for chaotic regimes with multiband structure.

\* Corresponding author. Fax: +7-8452-514549.

E-mail address: [pavlov@chaos.ssu.runnet.ru](mailto:pavlov@chaos.ssu.runnet.ru) (A.N. Pavlov).

Both the synchronous and the asynchronous regimes arising in the dynamics of coupled chaotic systems can be characterized by means of methods originating from Fourier analysis. This provides a possibility to determine the regions within which the effect of locking of the basic frequencies can be observed [9]. Another approach defines the instantaneous phases of interacting units [6] and follows the development of their difference. Numerical measures that can be used for diagnostic purposes include the spectrum of Lyapunov exponents, the diffusion coefficient of the phase difference, the mean return time to a Poincaré section [10], etc. Chaotic dynamics of evolutionary processes is reflected in the complex structure of their characteristic temporal scales, e.g., in the sequence of times when the phase space trajectory returns to a secant plane. Such sequences are sometimes related to a class of so-called multifractal objects [11]. They have different scaling properties for different subsets of the data and require a large number of characteristics to quantify their peculiarities. Multifractal phenomena are rather the rule than the exception in many areas of science [12]. They occur, for instance, in symbolic sequences [13] and medical data [14], in fully developed turbulence [15] and Brownian motion [16], in cloud structure [17], and in semiconductor diodes [18].

In this paper we investigate the scaling features of various processes in the evolutionary dynamics of two interacting chaotic oscillators. Taking coupled Rössler systems as a rather simple model demonstrating the period-doubling route to chaos we study how the transition to and between different types of synchronous motion is reflected in the structure of return times to a Poincaré section and to what extent scaling properties of return times can be applied to analyze complex phase dynamics. By means of two approaches, namely the wavelet transform modulus maxima (WTMM) method [16,19] and the detrended fluctuation analysis (DFA) [20], we investigate the scaling features of oscillations with different frequencies and with varying phase shift. We show that the transition from twomode asynchronous oscillations to a frequency-locked state can be studied in terms of the transition from multiscality to an almost monoscale sequence of return times. We discuss different types of correlations in the analyzed data and consider the influence of external noise.

## 2. Methods

### 2.1. WTMM-approach

The WTMM method originally proposed by Muzy et al. [19] is now one of the commonly used approaches to the study of multiscale structures in complex time series. Unlike the techniques used to estimate the  $f(x)$  singularity spectrum [11,21], the WTMM-approach is based on the wavelet transform method, which is a useful tool in the processing of nonstationary data. The attractiveness of using this technique is associated with the possibility it provides of analyzing a wide range of scales and a broad spectrum of scaling characteristics (from small fluctuations associated with weak singularities to large fluctuations and strong singularities). This is a clear advantage of the wavelet-based technique in comparison with the previously suggested structure function method [22] that investigates multiscale properties by calculating the moments of the probability density function. The WTMM-approach, described in details in [16], performs the numerical quantification of a time series by means of the so-called *singularity spectrum*  $D(h)$ , where  $D$  is the fractal dimension of the subset of the data characterized by the Hölder exponent  $h$ .

The applied algorithm involves two stages. At the first stage, the wavelet transform of a function  $f(x)$  is obtained:

$$T_\psi[f](x_0, a) = \frac{1}{a} \int_{-\infty}^{\infty} f(x) \psi\left(\frac{x-x_0}{a}\right) dx. \quad (1)$$

In practice, one often uses a random walk displacement for  $f(x)$  (the procedure of random walk building from experimental data is described below),  $a$  is the scale parameter, and  $\psi$  is the analyzing wavelet chosen, e.g., as the derivative of order  $m$  of a Gaussian function

$$\psi = \psi^{(m)} = (-1)^m \frac{\partial^m}{\partial x^m} \left[ \exp\left(-\frac{x^2}{2}\right) \right]. \quad (2)$$

If  $f(x)$  is a  $k$ -times continuously differentiable function at the point  $x_0$  then its wavelet coefficients satisfy to the following inequality:

$$T_\psi[f](x_0, a) \leq a^{k+1}, \quad a \rightarrow 0^+. \quad (3)$$

The scaling behavior of  $T_\psi[f]$  for an irregular function at the point  $x = x_0$  is described by the Hölder exponent  $h(x_0)$ :

$$T_\psi[f](x_0, a) \sim a^{h(x_0)}, \quad a \rightarrow 0^+. \quad (4)$$

All necessary information about a local singularity of  $f(x)$  including its localization  $x_0$  and the strength of the singularity  $h(x_0)$  can be obtained from the asymptotic behavior of the wavelet coefficients at small values of  $a$ . If these

coefficients are close to zero around the point  $x_0$  then  $f(x_0)$  is a regular function. The divergence of  $T_\psi[f](x, a)$  at small scales marks the presence of a local singular behavior at  $x = x_0$ . The corresponding value of the Hölder exponent can be found as the slope of the dependence of  $\ln T_\psi[f](x_0, a)$  vs.  $\ln a$  [23]. The estimated characteristic  $h(x_0)$  does not depend on the choice of the analyzing wavelet  $\psi$ . This is obviously an important aspect of the WTMM-approach. In our investigations the *Mexican hat* wavelet ( $m = 2$ ) was chosen for  $\psi$ .

At the second stage a partition function  $Z(q, a)$  is constructed representing the sum of  $q$ th powers of the local maxima of  $|T_\psi[f](x, a)|$  at the scale  $a$ . For small values of  $a$  the following power-law behavior is expected [16]:

$$Z(q, a) \sim a^{\tau(q)}, \tag{5}$$

where  $\tau(q)$  are the scaling exponents of  $Z(q, a)$ . The dependence  $\tau(q)$  is a linear function with the single Hölder exponent  $h(q) = d\tau/dq = \text{const.}$  for monofractal objects and a nonlinear function with a large number of exponents  $h(q)$  in the case of multifractals. The singularity spectrum  $D(h)$  can thereafter easily be estimated using the Legendre transform

$$D(h) = qh - \tau(q). \tag{6}$$

For positive values of  $q$  the partition function  $Z(q, a)$  characterizes the scaling of large fluctuations in the data series (strong singularities); for negative  $q$  it reflects the scaling of small fluctuations (weak singularities). Application of the WTMM-approach to time series allows us to characterize correlations of different types if  $h \neq 0.5$  and  $D(h) \neq 0$ . In particular, the range  $0 < h < 0.5$  implies the presence of anti-correlated behavior. This means that large (compared to the average) values of the data series are more probably to be followed by small values and vice versa [20].  $h > 0.5$  reflects correlated dynamics where large values are more likely to be followed by large values, and  $h = 0.5$  corresponds to uncorrelated behavior [14].

### 2.2. DFA-approach

A rather popular way to study the scaling features of time series consists in the use of the modified root mean square analysis of a random walk, termed DFA [20]. This approach allows us to quantify the scaling properties in processes of various origin. Numerical analysis of a time series  $z(i)$ ,  $i = 1, \dots, N$  within the framework of the DFA-technique is performed as follows. First, the mean value  $\bar{z}$  is removed from  $z(i)$  and the resulting time series is integrated to obtain the random walk  $y(k) = \sum_{i=1}^k [z(i) - \bar{z}]$ . Next,  $y(k)$  is divided into time windows of length  $n$ , from each of which the local linear trend  $y_n(k)$  is subtracted [20]. It is expected that the root mean square fluctuations  $F(n)$ ,

$$F(n) = \sqrt{\frac{1}{N} \sum_{k=1}^N [y(k) - y_n(k)]^2} \tag{7}$$

show the power-law dependence  $F(n) \sim n^\alpha$ . In practice,  $\alpha$  can be found as the slope of the line relating  $\lg F$  to  $\lg n$ . These slopes may not coincide for different scaling regions. That is why an analysis of local exponents may be used to characterize the detailed structure of complex time series. Like the Hölder exponents of the WTMM-method, the numerical values of  $\alpha$  indicate the presence of uncorrelated behavior if  $\alpha = 0.5$ . (In this case the local slopes may be different from 0.5 for small  $n$  at the presence of only short-term correlations however  $\alpha$  approaches 0.5 for large  $n$ .) The range  $0.5 < \alpha < 1$  corresponds to power-law correlations while the range  $0 < \alpha < 0.5$  reflects the presence of anti-correlations in data series (and the smaller  $\alpha$  is the more probable is the alternation between large and small values). The special case  $\alpha = 1$  is related to  $1/f$ -noise. For  $\alpha > 1$  correlations also exist, however they are not of a power-law form [20].

### 3. Model

Let us consider a system of two coupled Rössler oscillators as described in [6]:

$$\begin{aligned} \frac{dx_{1,2}}{dt} &= -\omega_{1,2}y_{1,2} - z_{1,2} + c(x_{2,1} - x_{1,2}), \\ \frac{dy_{1,2}}{dt} &= \omega_{1,2}x_{1,2} + \alpha y_{1,2}, \\ \frac{dz_{1,2}}{dt} &= \beta + z_{1,2}(x_{1,2} - \mu). \end{aligned} \tag{8}$$

This system can serve as a simple model, allowing us to study the transitions to and between various types of synchronous and asynchronous dynamics. Here, the parameters  $\alpha$ ,  $\beta$ , and  $\mu$  govern the dynamics of each subsystem, and

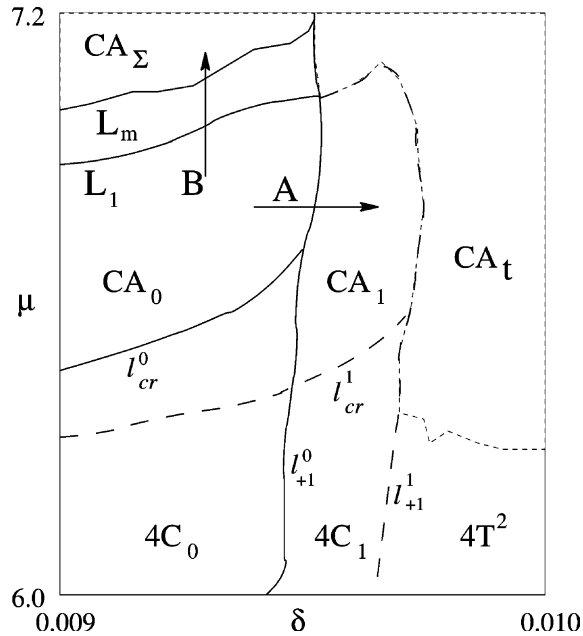


Fig. 1. Bifurcation diagram for two coupled Rössler systems. Only bifurcational curves that are of interest for the further analysis are indicated here. A more detailed diagram is given in [8]. The diagram illustrates the effects of phase multistability.

$c$  is the coupling parameter.  $\omega_1 = \omega_0 + \delta$  and  $\omega_2 = \omega_0 - \delta$  are the basic frequencies of the two subsystems and  $\delta$  is the mismatch between them. The parameters are chosen as follows:  $\alpha = 0.15$ ,  $\beta = 0.2$ ,  $c = 0.02$ , and  $\omega_0 = 1.0$ . A bifurcation analysis of Eq. (8) was performed by Postnov et al. [8]. Let us briefly recall those aspects of their bifurcation diagram on the  $(\delta, \mu)$  parameter plane (Fig. 1) that are necessary for the further discussion.

The interactive dynamics of two Rössler oscillators leads to the appearance of a variety of periodic and chaotic solutions related to different attractor families with distinct phase shift. We consider here only two families having the largest basins of attraction, namely, “in-phase” and “out-of-phase” attractors [8]. In the first case the phase difference of  $x_1(t)$  and  $x_2(t)$  vanishes for  $\omega_1 = \omega_2$  (the corresponding periodic regimes are labeled as  $2^i C_0$ , where  $i = 1, 2, 3, \dots$ , and  $2^i$  denotes the cycle period). In the second case the phase difference for the subharmonic components takes the value  $2\pi$  (the attractors are denoted as  $2^i C_1$ ).

Fig. 1 shows some of the bifurcational curves in the  $(\delta, \mu)$  parameter plane:  $l_{+1}^j$  ( $j = 0, 1$ ) are the curves of tangent bifurcations of cycles  $2^i C_j$  (edges of Arnol’d tongues);  $l_{cr}^j$  are the critical curves where accumulation of the period-doubling cascades for  $2^i C_j$  cycles takes place. Below  $l_{cr}^j$  periodic attractors of “in-phase” and “out-of-phase” families demonstrate the period-doubling route to chaos (to simplify the bifurcation diagram we do not present the details of this route). As a consequence, chaotic regimes  $CA_0$  and  $CA_1$  appear. At the curve  $L_1$ , the  $CA_1$  family undergoes a boundary crisis and turns into a chaotic saddle. Increasing  $\mu$  leads to the merging of the chaotic attractor  $CA_0$  with the saddle  $CA_1$  at  $L_m$ . The resulting attractor is denoted as  $CA_\Sigma$  and is characterized by two positive Lyapunov exponents. The curve  $l_{+1}^1$  denotes the boundary of the synchronization region. To the right of this curve quasiperiodic oscillations  $4T^2$  and asynchronous chaotic dynamics  $CA_t$  take place.

In Section 4 we shall discuss how the transitions from synchronous ( $CA_j$ ) to asynchronous ( $CA_t$ ) chaotic dynamics (direction A in Fig. 1) and from chaos ( $CA_j$ ) to hyperchaos ( $CA_\Sigma$ ) along the direction B are reflected in the fractal structure of the return times to a Poincaré section.

#### 4. Analysis of return times

##### 4.1. Direction A: transition from synchronous to asynchronous oscillations

Before we discuss the transition from the synchronous chaotic attractor  $CA_0$  (or  $CA_1$ ) to the asynchronous attractor  $CA_t$ , in detail let us look for a moment at the shapes of their singularity spectra  $D(h)$  calculated from sequences of return

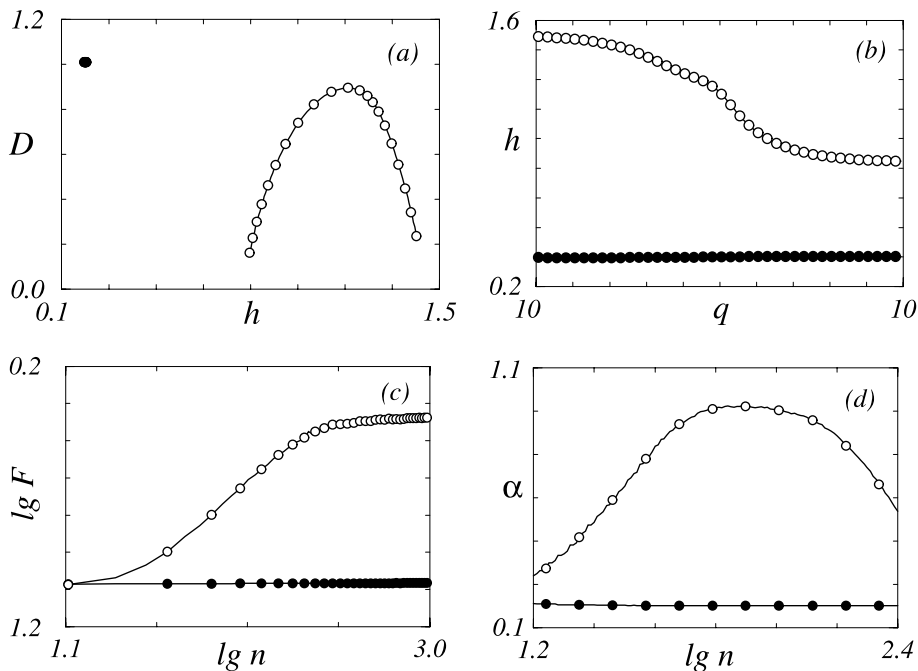


Fig. 2. Scaling properties of the synchronous chaotic attractor  $CA_0$  ( $\mu = 6.8$ ,  $\delta = 0.00934$ , black circles) and the asynchronous attractor  $CA_t$  ( $\mu = 6.8$ ,  $\delta = 0.00988$ , white circles): (a,b) singularity spectra  $D(h)$  and Hölder exponents  $h(q)$  of the WTMM-approach; (c,d) root mean square fluctuations  $F(n)$  (in double logarithmic plot) and local scaling exponents  $\alpha$  of the DFA-technique.

times to the Poincaré section  $x_2 = 0$  (Fig. 2a). They show two remarkable distinctions: (i) The values of the Hölder exponents  $h(0)$  that are related to the maxima of the singularity spectra ( $q = 0$ ) do not coincide for the two attractors; (ii) the width of the singularity spectrum for the asynchronous regime  $CA_t$  is significantly larger than for  $CA_0$ . This means that the transition from  $CA_0$  to  $CA_t$  can be described in terms of the transition from an almost monofractal (or monoscale) structure of the return time sequence characterized by a practically linear dependence  $\tau(q)$  and by an almost constant value of  $h(q)$  (Fig. 2b, black circles) to a multifractal (multiscale) structure that requires a large number of Hölder exponents to characterize its scaling properties (Fig. 2b, white circles). We speak here about an *almost* monoscale structure for  $CA_0$  because it is rather difficult (or even impossible) to compute a singularity spectrum consisting nearly of a single point. Estimation of the Hölder exponents for large numerical values of  $q$  is typically sensitive to computational parameters like the range used for fitting the scaling exponents  $\tau(q)$ . In some situations it is unclear whether the analyzed object can be related to a class of monofractals. This is why it will be probably more correct to speak about the degree of multifractality. Because the maximal values of the fractal dimensions  $D$  do not show significant differences within the framework of the WTMM-approach (they are both close to 1 for the chosen regimes) in the further discussion we will consider only changes in the spectrum of Hölder exponents  $h(q)$  instead of shapes of  $D(h)$ .

Similar conclusions follow from the DFA-analysis: the dependence of  $\lg F$  vs.  $\lg n$  is close to a constant for  $CA_0$  (Fig. 2c, black circles). Hence, the local scaling exponents  $\alpha$  practically coincide at  $\alpha \approx 0.01$  (Fig. 2d). However, this situation changes dramatically in the case of asynchronous chaos (Fig. 2c and d). We can see from Fig. 2d that the local values of  $\alpha$  vary significantly for the considered regimes and are close to 1.0 (the case of  $1/f$ -noise) in an interval around  $\lg n = 2.0$ .

Fig. 3 demonstrates the results of more detailed investigations of the transition  $CA_1 \rightarrow CA_t$  when we use the Poincaré section  $x_2 = 0$ . The appearance of asynchronous dynamics under variation of the control parameter  $\delta$  is clearly diagnosed by both the DFA-technique (Fig. 3a) and the WTMM-approach (Fig. 3b). In Fig. 3 we have denoted the range of scaling exponents obtained by the DFA as  $\Delta_x$ , i.e.,  $\Delta_x$  is the difference between the maximal and the minimal values of local scaling characteristics;  $\bar{x}$  is the mean value. By analogy,  $\Delta_h$  is the range of Hölder exponents. Rather similar dependences can be obtained for other secant planes ( $x_1 = 0$ ,  $y_1 = 0$ , and  $y_2 = 0$ ). The DFA shows that the asynchronous regime  $CA_t$  is characterized by a value  $\bar{x} > 0.5$ , corresponding to the presence of power-law correlations in the

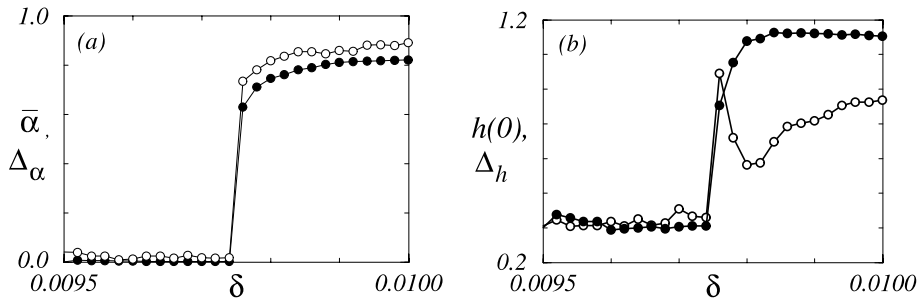


Fig. 3. Scaling characteristics along the direction A ( $\mu = 6.8$ ): (a) mean values of the scaling exponents of the DFA-approach (black circles) and the ranges  $\Delta_x$  (white circles); (b) Hölder exponents corresponding to maxima of the singularity spectra (black circles) and the ranges  $\Delta_h$  (white circles). Synchronous dynamics is characterized by strong anti-correlations of the return-time sequences whereas the statistical properties of asynchronous chaos demonstrate correlated behavior (close to  $1/f$ -noise in some interval of scales).

data series. But  $\bar{\alpha}$  is close to zero for the attractors  $CA_0$  and  $CA_1$ , indicating strong anti-correlations. We can therefore conclude that increasing the control parameter  $\delta$  along the direction A changes the type of correlations in the return time sequences and results in a strong enhancement of different measures describing multiscale properties ( $\Delta_x$  and  $\Delta_h$  in Fig. 3).

We should emphasize, of course, that the series of return times for synchronous oscillations cannot always be characterized in terms of monoscale objects. In particular the range of Hölder exponents for the chaotic regime  $CA_1$  can be somewhat wider than for  $CA_0$  (Fig. 4a). However, this range is still small when compared with the state of asynchronous chaos  $CA_r$ . This is why we can generally describe synchronous oscillations in the dynamics of coupled Rössler systems as a regime with significantly smaller degree of multiscale properties than complex motions outside the synchronization region. The effect of decreasing the multiscale properties was recently observed also for stochastic resonance [24]. By comparison with the WTMM-method that in principle allows us to distinguish between the attractors  $CA_0$  and  $CA_1$  (although such a distinction between various regimes of a phase multistability is not always possible), the DFA-technique appears to be a less appropriate tool because the transition  $CA_0 \rightarrow CA_1$  is not well expressed in the structure of return times. However, the DFA-approach, being a relatively easy numerical method, provides us with the possibility to clearly distinguish between the synchronous ( $CA_j$ ) and the asynchronous ( $CA_r$ ) dynamics when computing the range of scaling characteristics  $\Delta_x$ . For the considered case we have seen that this distinction (Fig. 3a) is perhaps even better than for the measure  $\Delta_h$  of the wavelet-based technique (Fig. 3b). That is why we think that a simultaneous application and comparison of both approaches may be useful to quantify the complex structure of the analyzed data.

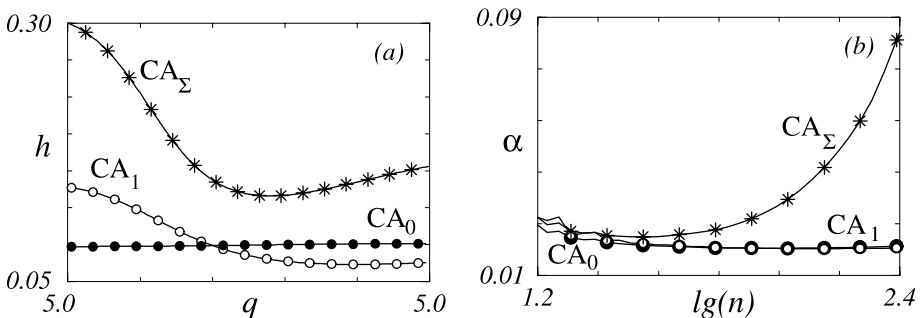


Fig. 4. WTMM (a) and DFA (b) scaling characteristics for three different synchronous regimes.  $\mu = 6.7$ ,  $\delta = 0.0094$  for  $CA_0$  and  $CA_1$  and  $\mu = 7.2$ ,  $\delta = 0.0093$  for  $CA_\Sigma$ . The hyperchaotic attractor  $CA_\Sigma$  requires a wider range of scaling characteristics than the synchronous attractors  $CA_0$  and  $CA_1$ . DFA-approach show that statistical properties of chaotic dynamics are close enough when considering short- and middle-term anti-correlations (the window size  $n < 50$ ). However, long-term anti-correlations ( $n > 100$ ) are characterized by obviously different scaling exponents.

#### 4.2. Direction B: transition from chaos to hyperchaos

With increasing parameter  $\mu$  (direction B in Fig. 1), a band-merging bifurcation of the chaotic attractors  $CA_0$  and  $CA_1$  leads to the appearance of a new regime  $CA_\Sigma$ . The attractor  $CA_\Sigma$  contains the trajectories of  $CA_0$  and  $CA_1$  and has two positive Lyapunov exponents [8]. Therefore, hyperchaotic oscillations takes place. The transition  $CA_1 \rightarrow CA_\Sigma$  (or  $CA_0 \rightarrow CA_\Sigma$ ) also leads to changes of the scaling properties that can be detected by the DFA-approach (Fig. 4b). Although the local exponents of the DFA are fairly small in both cases indicating the presence of strong anti-correlations in the data series, their dependences on the window size  $n$  used for linear fit of the local trend are quite different. The hyperchaotic dynamics  $CA_\Sigma$  requires a wider range of scaling characteristics  $\Delta_\alpha$  than the attractors  $CA_0$  and  $CA_1$  (Fig. 4b).

The changes of the return time structure that take place under variation of the parameter  $\mu$  were examined by the wavelet-based technique. The values of  $\Delta_h$  can differ approximately by a factor of two for  $CA_1$  and  $CA_\Sigma$  (Fig. 4a). Besides this, the Hölder exponents  $h(q)$  take larger values in the hyperchaotic regime. An increase of the scaling characteristics  $h(q)$  and  $\bar{\alpha}$  at the transition  $CA_j \rightarrow CA_\Sigma$  again reflects the changes of power-law correlations in the return times. The values  $\alpha \approx h \approx 0$  correspond to strong anti-correlations that become weaker for the attractor  $CA_\Sigma$ . Fig. 5 demonstrates the results of more detailed investigations of the transition  $CA_j \rightarrow CA_\Sigma$ . As a quantitative measure describing the multiscale properties we have chosen here the range of local exponents of the DFA-technique  $\Delta_\alpha$ .

A comparison of various transitions arising at the interaction of two coupled Rössler systems shows that the asynchronous attractors are clearly distinguished from the synchronous ones (Fig. 6). In particular, the transition  $CA_\Sigma \rightarrow CA_i$  under variation of the mismatch parameter is similar to that in Fig. 3. At the same time, following the results presented in Fig. 6, an analysis of the scaling properties can provide a diagnostics of different dynamical regimes such as inside the synchronization region ( $CA_0$  and  $CA_\Sigma$ ) and outside this region ( $4T^2$  and  $CA_i$ ). Below the curve  $h(q)$  for the attractor  $CA_\Sigma$  other spectra of Hölder exponents for various synchronous regimes (chaotic or periodic) could be drawn (we omit them here because these curves practically coincide with  $h(q)$  for  $CA_0$ ).

#### 4.3. Scaling properties of return times at the presence of noise

Let us consider the changes of the return time structure caused by the influence of noise. For this purpose we have included Gaussian white noise additively to the first equation of the coupled Rössler oscillators (8), i.e., we have added a term  $I\xi(t)$ , where  $I$  is the intensity of normally distributed random process. Because external fluctuations can lead to intermittency between coexisting regimes it is expected that the scaling properties of the noisy dynamics will not be the same as for the deterministic case. Numerical calculations testify this. In particular, the behavior of the scaling characteristics at the transition from synchronous to asynchronous motion is smeared out, without clearly expressed “jumps” (Fig. 7) that could serve as indicators of the boundary of the synchronization region (compare with Fig. 3).

A high sensitivity to external fluctuations arises even in the case of co-existing periodic oscillations. Such regimes do not have fractal properties in the case of deterministic motions ( $\alpha = h = 0$ ), however, the process of intermittency between different periodic attractors caused by the noise can result in strong multifractality of the return time dynamics as it can be shown by the WTMM-technique (Fig. 8) as well as by the DFA.

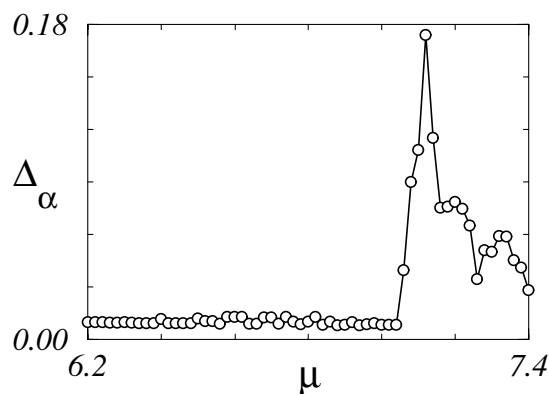


Fig. 5. Range of local scaling exponents  $\Delta_\alpha$  vs. parameter  $\mu$  for  $\delta = 0.0093$ . We note the transition to a merged attractor at  $\mu \approx 7.05$ .

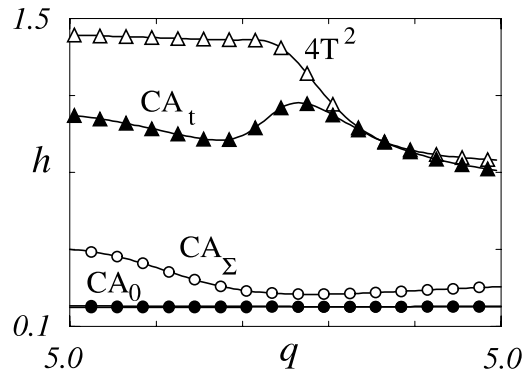


Fig. 6. Hölder exponents for synchronous (○) and asynchronous (△) dynamics.  $\mu = 6.7$ ,  $\delta = 0.0094$  for  $CA_0$ ,  $\mu = 7.2$ ,  $\delta = 0.0093$  for  $CA_\Sigma$ ,  $\mu = 6.8$ ,  $\delta = 0.0098$  for  $CA_t$ , and  $\mu = 6.2$ ,  $\delta = 0.0098$  for  $4T^2$ .

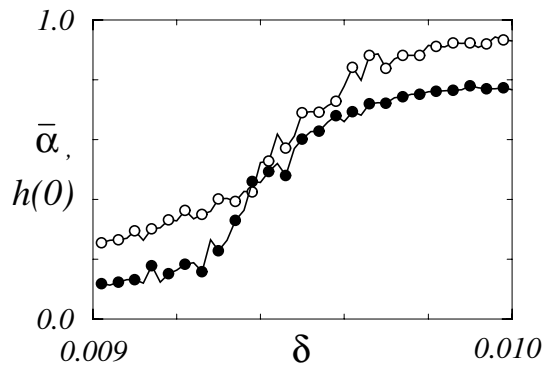


Fig. 7. Scaling characteristics  $\bar{\alpha}$  (white circles) and  $h(0)$  (black circles) vs. the control parameter  $\delta$  in the case of stochastic dynamics ( $\mu = 6.8$ ,  $I = 10^{-1}$ ).

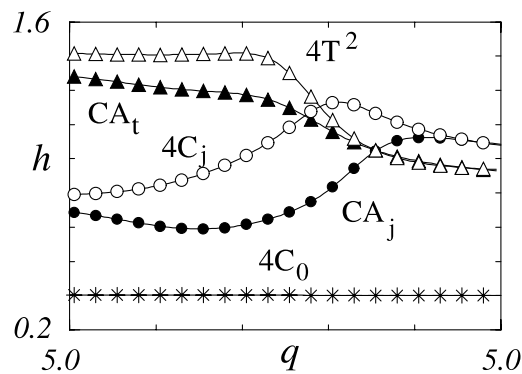


Fig. 8. Scaling properties of stochastic synchronous (○) and asynchronous (△) motions ( $I = 10^{-1}$ ). Here, the notations  $4C_j$  and  $CA_j$  refer to the process of intermittency between the corresponding periodic or chaotic attractors caused by noise. Stars correspond to periodic oscillations  $4C_0$  at the absence of fluctuations ( $\delta = 0.0093$ ,  $\mu = 6.2$ ). Parameter values for other regimes are the same as in Fig. 6.

Chaotic regimes inside the synchronization region are also rather sensitive to fluctuations. The scaling exponents  $h(q)$  or  $\alpha(n)$  in this case can be close to the characteristics of the intermittency process between periodic regimes given in

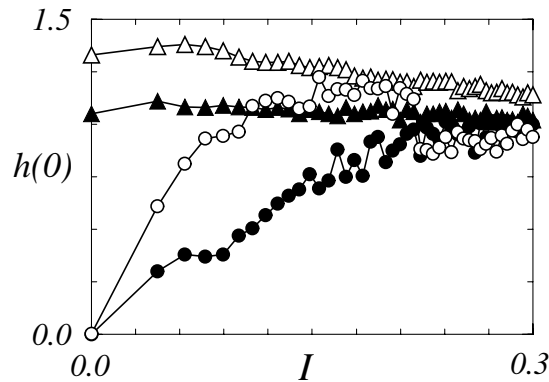


Fig. 9. Scaling properties of stochastic motions vs. noise intensity  $I$ . All denotations and parameter values are the same as in Fig. 8.

Fig. 8. As a result, it may be impossible to distinguish between different types of noisy dynamics. But, if the intensity of a normally distributed random process is relatively low (say,  $<10^{-1}$ ) and we do not consider a neighborhood of the boundary of the synchronization region then the scaling properties of synchronous and asynchronous dynamics obviously do not coincide for negative  $q$  (Fig. 8). Note that according to Fig. 8 the direction A does not manifest a transition from monoscale to multiscale structure in the case of noisy dynamics and even the opposite effect (decreasing multiscale properties) may be observed in numerical experiments. With increasing noise intensity the scaling properties of various stochastic motions becomes very similar (Fig. 9).

## 5. Conclusions

Interactive dynamics of two coupled chaotic oscillators can produce a variety of phase-locked and multistable regimes. These regimes have different metrical and dynamical properties and can be characterized by various mathematical approaches. Complex dynamics of interacting units is usually reflected in the complex structure of typical temporal scales (like return times, for instance). To quantify this structure we considered two well-known techniques, namely, the WTMM method and DFA. Both approaches are rather universal tools of processing experimental data that can be applied independently on whether the analyzed time series is stationary or not.

By studying regimes with different phase and frequency properties inside and outside the synchronization region, in the case of deterministic dynamics we demonstrated that the transition from asynchronous to synchronous motion reduces the degree of multiscale structure of the dynamic processes. Sometimes it can even be described as a transition from a multiscale structure of the return times to an almost monoscale structure. Regimes inside the synchronization region corresponding to the case of a phase multistability can be distinguished using the scaling characteristics of the WTMM-method. However, the differences are fairly small. Merging of the chaotic attractors  $CA_0$  and  $CA_1$ , leading to a hyperchaotic dynamics  $CA_\Sigma$ , resulted in some increase of the scaling exponents of the DFA-approach. This means that the strong anti-correlations in the return times that exists for the attractors  $CA_0$  and  $CA_1$  becomes weaker for  $CA_\Sigma$ .

External fluctuations lead to more complicated dynamics of the coupled Rössler systems. Fluctuations reduced the differences between the various types of synchronous motion and removed the clearly expressed boundary of the synchronization region. However, if the noise intensity is reasonably low the synchronous and asynchronous motions can still be distinguished using the spectrum of Hölder exponents of the wavelet-based technique because the considered regimes demonstrate different scaling for negative values of  $q$  related to small fluctuations (weak singularities) in data series.

## Acknowledgements

This work was supported by the Danish Natural Science Foundation and INTAS 01-2061. A.P. acknowledges the support of CRDF (Award REC-006). O.S. acknowledges INTAS (grant YSF 01/1-0023).

## References

- [1] Kuramoto Y. *Chemical oscillations, waves and turbulence*. Berlin: Springer-Verlag; 1984.
- [2] Pikovsky A, Rosenblum M, Kurths J. *Synchronization: a universal concept in nonlinear sciences*. In: Cambridge nonlinear science series 12. Cambridge University Press; 2001.
- [3] Mosekilde E, Maistrenko Yu, Postnov D. *Chaotic synchronization: applications to living systems*. Singapore: World Scientific; 2002.
- [4] Fujisaka H, Yamada Y. *Progr Theor Phys* 1983;69:32;  
Afraimovich VS, Verichev NN, Rabinovich MI. *Radiophys Quantum Electron* 1986;29:795;  
Pecora LM, Carroll TL. *Phys Rev Lett* 1990;64:821.
- [5] Rosenblum MG, Pikovsky AS, Kurths J. *Phys Rev Lett* 1997;78:4193.
- [6] Rosenblum MG, Pikovsky AS, Kurths J. *Phys Rev Lett* 1996;76:1804.
- [7] Rulkov NF, Sushchik MM, Tsimring LS, Abarbanel HDI. *Phys Rev E* 1995;51:980;  
Kocarev L, Parlitz U. *Phys Rev Lett* 1996;76:1816.
- [8] Postnov DE, Vadivasova TE, Sosnovtseva OV, Balanov AG, Anishchenko VS, Mosekilde E. *Chaos* 1999;9:227;  
Vadivasova TE, Sosnovtseva OV, Balanov AG, Astakhov VV. *Discrete Dyn Nat Sci* 2000;4:231.
- [9] Anishchenko VS, Vadivasova TE, Postnov DE, Safonova MA. *Int J Bifurcat Chaos* 1992;2:633.
- [10] Vadivasova TE, Balanov AG, Sosnovtseva OV, Postnov DE, Mosekilde E. *Phys Lett A* 1999;253:66.
- [11] Halsey TC, Jensen MH, Kadanoff LP, Procaccia I, Shraiman BI. *Phys Rev A* 1986;33:1141;  
*Tel T. Z Naturforsch* 1988;43a:1154;  
Jensen MH, Paladin G, Vulpiani A. *Phys Rev Lett* 1991;67:208.
- [12] Mandelbrot BB. In: *Fractals and multifractals: noise, turbulence and galaxies, selecta*, Vol. 1. New York: Springer-Verlag; 1989;  
Bunde A, Havlin S, editors. *Fractals in science*. Berlin: Springer; 1994;  
Kantz H, Schreiber T. *Nonlinear time series analysis*. In: Cambridge nonlinear science series 7. Cambridge University Press; 1997.
- [13] Berthelsen CL, Glazier JA, Raghavachari S. *Phys Rev E* 1994;49:1860;  
Strait BJ, Dewey TG. *Phys Rev E* 1995;52:6588.
- [14] Ivanov PCh, Amaral LAN, Goldberger AL, Havlin S, Rosenblum MG, Struzik ZR, et al. *Nature* 1999;399:461.
- [15] Benzi R, Biferale L, Paladin G, Vulpiani A, Vergassola M. *Phys Rev Lett* 1991;67:2299.
- [16] Muzy JF, Bacry E, Arneodo A. *Int J Bifurcat Chaos* 1994;4:245.
- [17] Arrault J, Arneodo A, Davis A, Marshak A. *Phys Rev Lett* 1997;79:75.
- [18] Mosekilde E, Thomsen JS, Knudsen C, Feldberg R. *Physica D* 1993;66:143.
- [19] Muzy JF, Bacry E, Arneodo A. *Phys Rev Lett* 1991;67:3515.
- [20] Buldyrev SV, Goldberger AL, Havlin S, Peng C-K, Simons M, Stanley HE. *Phys Rev E* 1993;47:4514;  
Peng C-K, Havlin S, Stanley HE, Goldberger AL. *Chaos, Solitons & Fractals* 1995;5:82.
- [21] Jensen MH, Kadanoff LP, Libchaber A, Procaccia I, Stavans J. *Phys Rev Lett* 1985;55:2798.
- [22] Frish U, Parisi G. In: Ghil M, Benzi R, Parisi G, editors. *Turbulence and predictability in geophysical fluid dynamics and climate dynamics*. Amsterdam: North-Holland; 1985. p. 71.
- [23] Mallat S, Hwang WL. *IEEE Trans Inf Theory* 1992;38:617.
- [24] Silchenko A, Hu C-K. *Phys Rev E* 2001;63:041105.